Associations Between Blood Markers of the GSH Redox cycle and Brain White Matter Microstructure in Psychosis

Tommaso Pavan, Pascal Steullet, Yasser Alemán-Gómez, Raoul Jenni, Zoé Schilliger, Martine Cleusix, Luis Alameda, Kim Q. Do, Philippe Conus, Patric Hagmann, Daniella Dwir, Paul Klauser, Ileana Jelescu

August 12, 2024

Supplementary Material

Methods details

Acquisition details

Magnetization-prepared rapid acquisition gradient echo (MPRAGE): echo time (TE) 2.98ms, repetition time (TR) 2300 ms, inversion time (TI) 900 ms, field of view (FOV) 160 x 240 x 256 mm^3 and voxel size 1 x 1 x 1.2 mm^3), acquisition time 7 minutes. Pulsed Gradient Spin-echo (PGSE) echo planar imaging (EPI) sequence: acquired in cartesian q-space coverage totalling 129 (Prisma) or 257 (Trio) DWI volumes. Prisma: TE = 144 ms, TR = 6.1 s; Trio: TE = 103 ms, TR = 5.9 s. FOV = 211 x 211 x 114mm^3, voxel size = 2.2 x 2.2 x 3mm^3, 96x96x38 slices, partial Fourier = 0.75, 1 b0 acquisition 128 (Prisma) and 256 (Trio) directions, acquisition time 13 minutes. Any participants with pacemaker, cochlear implant, implant of stimulator or drug pump, glucose sensor, bypass valve or pregnant were not allowed in the MRI scanner and excluded from the study.

Preprocessing details

The diffusion preprocessing pipeline included MP-PCA denoising (Veraart et al., 2016) and Gibbs ringing correction (Kellner et al., 2016; Lee et al., 2021). The EPI distortions were corrected using ANTs non-linear registration since no reverse phase encode image or magnetic field map were acquired. The registration of the DSI b=0 volume to the MPRAGE was constrained only in the direction of the distortion, for then warping the estimated correction back to each DWI volume in native space (Alemán-Gómez et al., 2023; Tax et al., 2022). Thereafter, the distortion-corrected images were further corrected for eddy currents and motion using FSL *eddy* (Andersson and Sotiropoulos, 2016). Since FSL eddy does not support DSI data natively (see *–data_is_shelled* in: https://fsl.fmrib.ox.ac.uk/fsl/fslwiki/eddy/UsersGuide), temporarily merging or directly dropping a subset of volumes

based on their b-values in order to simulate shells was necessary to accommodate the algorithm. Namely, volumes b=1500 and b=2000 were merged as b=1750, b=4000 was merged to b=4500 while b=6000 and b=8000 were removed. Right after the eddy execution the merged volumes were split back into their original b-values except for the dropped volumes (for the dMRI metric estimations only the b-values$\leq$2500 were needed). The reduced DWI images featured 29 and 57 directions (Prisma, 1:b=0, 3:b=500, 6:b=1000, 4:b=1500, 3:b=2000, 12:b=2500; Trio, 1:b=0, 6:b=500, 12:b=1000, 8:b1500, 6:b=2000, 24:b=2500). Data quality was assessed by visual inspection and automated means (FSL's eddy QUAD and SQUAD (Bastiani et al., 2019)). The estimated quality metrics were volume-to-volume (absolute movement) and within-volume motion (relative movement), eddy current-induced distortions and data outliers. For the Trio scanner the study mean absolute movement was 1.08 ± 0.39 mm [min:0.21, max:3.21]; while the mean relative movement was 0.02 ± 0.013 mm [min:0, max:0.1]. For the Prisma scanner the study mean absolute movement was 0.46 ± 0.31 mm [min:0.13, max:3.36]; while the mean relative movement was 0.1 ± 0.06 mm [min:0.02, max:0.61].

Blood sample details

GR activity was assessed in hemolyzed blood cells incubated in phosphate buffer solution (100mM, pH 7.5) containing EDTA (0.6mM), and non-limiting levels of oxidized glutathione (GSSG, 2.5mM) and NADPH (0.25mM). The activity of GR was expressed as the amount of NADPH used by GR (in nmole/min at 22°C) to reduce GSSG. The decrease of NADPH was measured using the decrease of absorption at 340 nm (per min) and quantified using the NADPH 340 nm absorption coefficient. GPx activity was assessed in hemolyzed blood cells incubated in a phosphate buffer solution (100mM, pH 7.5) with EDTA (0.6mM), and non-limiting amounts of GSH (2.5mM), NADPH (0.25mM), GR (0.84U/ml; Fluka) and tert-butyl hydroperoxide (TBHP, 0.8mM, Fluka). The activity of GPx is proportional to the amount of NADPH used to reduce the GSSG produced during the reduction of TBHP by GPx. The decrease of NADPH was measured using the decrease of absorption at 340 nm (per min) and quantified using the NADPH 340nm absorption coefficient.

Reader harmonization

To correct for the batch effect of the two microplate reader, the ComBat method from the R (R Core Team, 2023) package Surrogate Variable Analysis (SVA, Leek et al. (2012)) was used. GPx and GR values were harmonized together and we specified age, sex and clinical group as model matrix for outcome of interest so that the effect of the specified variables could be protected from accidental corrections. To assure the correction was working we compared the results obtained to the original data and the data normalized by reader type (demeaned and scaled by the standard deviation, see Fig. S 1 and 2). We observed that, despite the normalization already accounts for a large amount of the differences between the readers, the harmonization procedure better preserves the the relation within the reader group (in Fig. S 1 and 2, subplots G vs H).

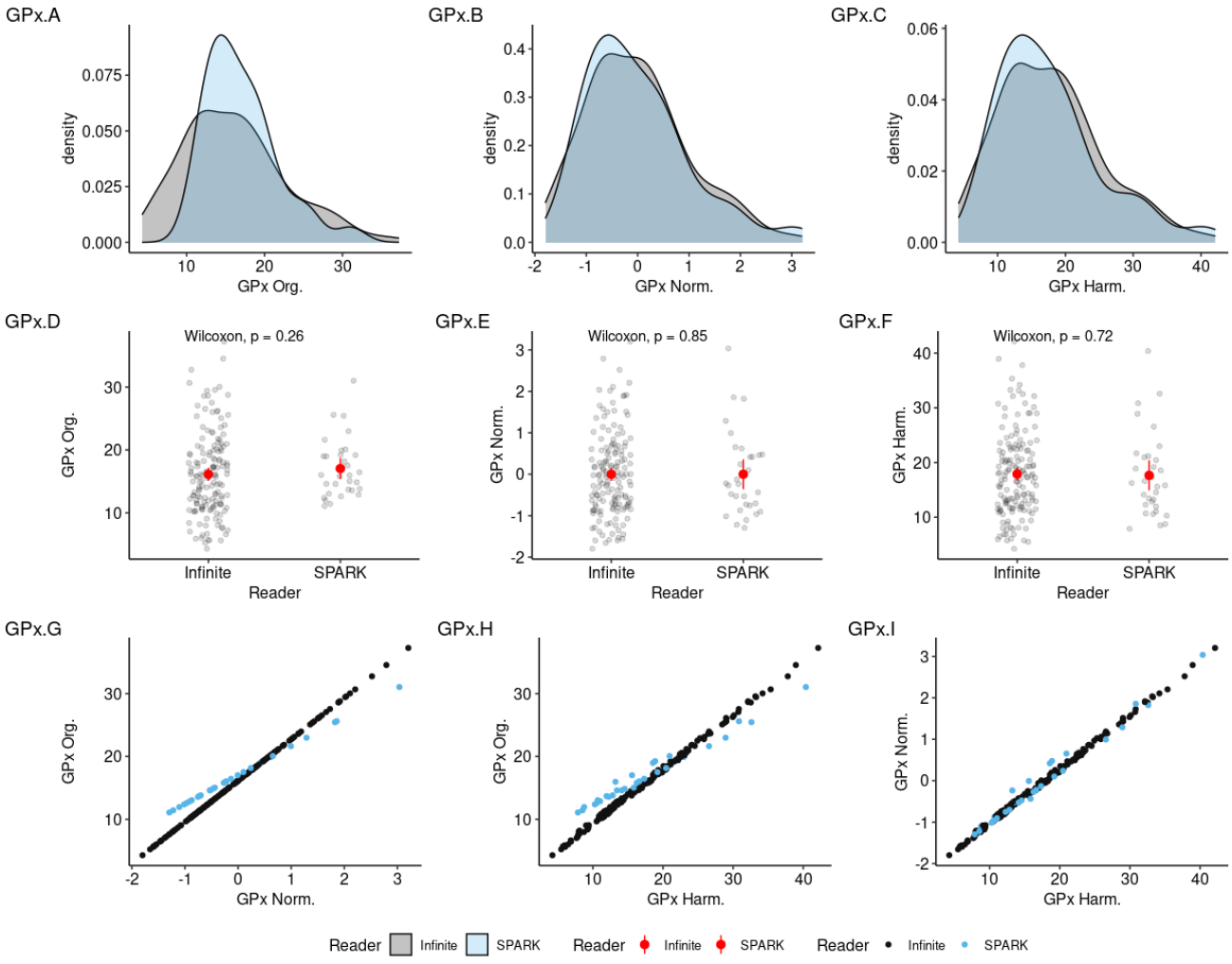

Figure S 1: comparison between GPx original data, normalization and harmonization. GPx distributions for original data (A), normalized by scanner (B) and harmonized (C). Group comparison between the readers of original data (D), normalized by scanner (E) and harmonized (F). Relation between original and normalized GPx data (G), between original and harmonized GPx data (H), between normalized and harmonized GPx data (I). Org.: Original; Norm.: normalised; Harm.: harmonized.

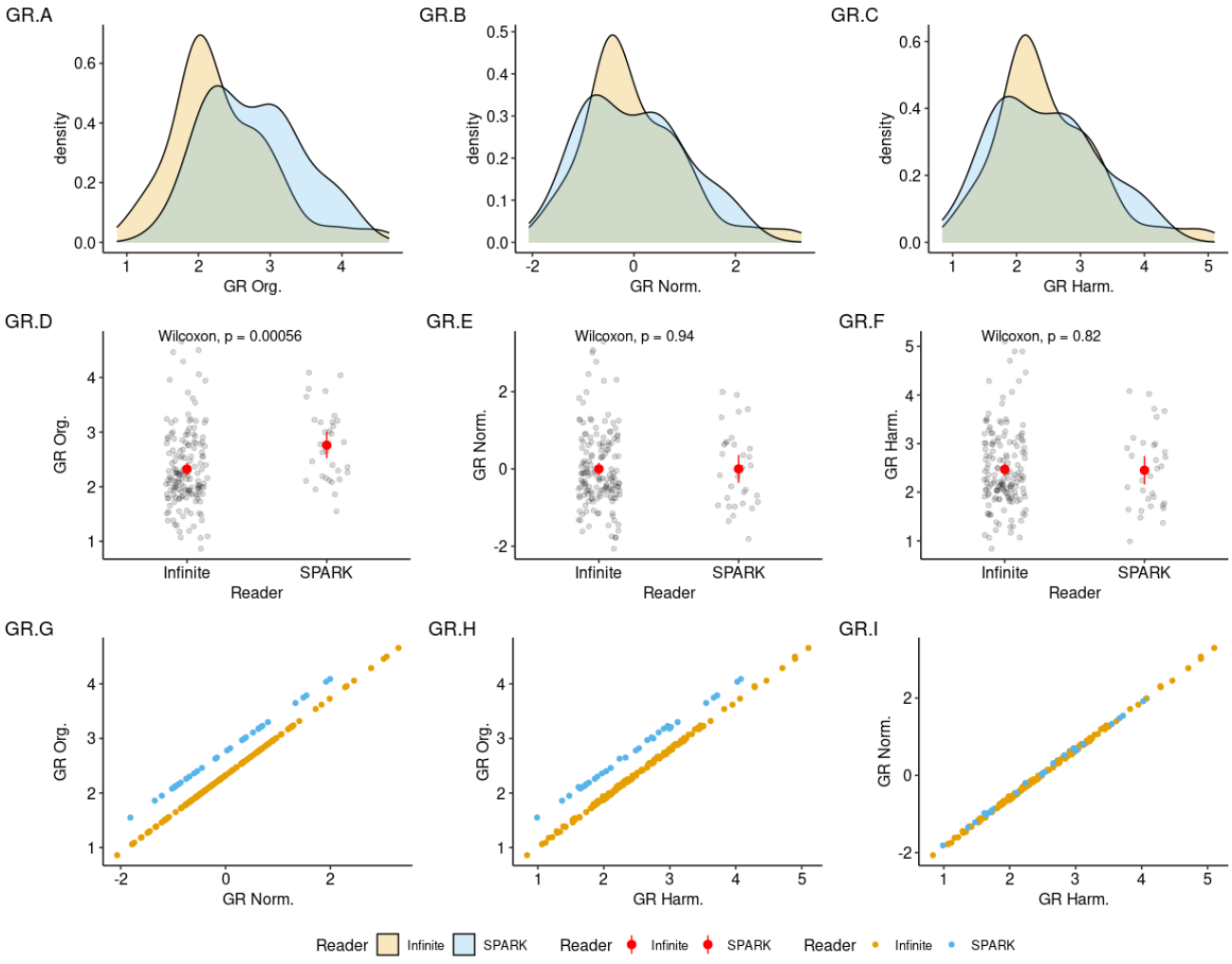

Figure S 2: comparison between GR original data, normalization and harmonization. GR distributions for original data (A), normalized by scanner (B) and harmonized (C). Group comparison between the readers of original data (D), normalized by scanner (E) and harmonized (F). Relation between original and normalized GR data (G), between original and harmonized GR data (H), between normalized and harmonized GR data (I). Org.: Original; Norm.: normalised; Harm.: harmonized.

Age correction

To better model age and correct for its effect, five different model were evaluated for each of the 4 WM skeletons metric: no age effect (intercept-only), linear age effect (LAE), quadratic age effect (QAE), linear age effects with group interaction (LAEG) and quadratic age effects with group interaction (QAEG); for a total of 16 models. The model selection criteria was to minimize the Bayesian information criterion (BIC) between the fitted model for one metric, and then selecting the most popular correction model among the metrics. The procedure returned the QAE as the best model. See Figure S3 for an example.

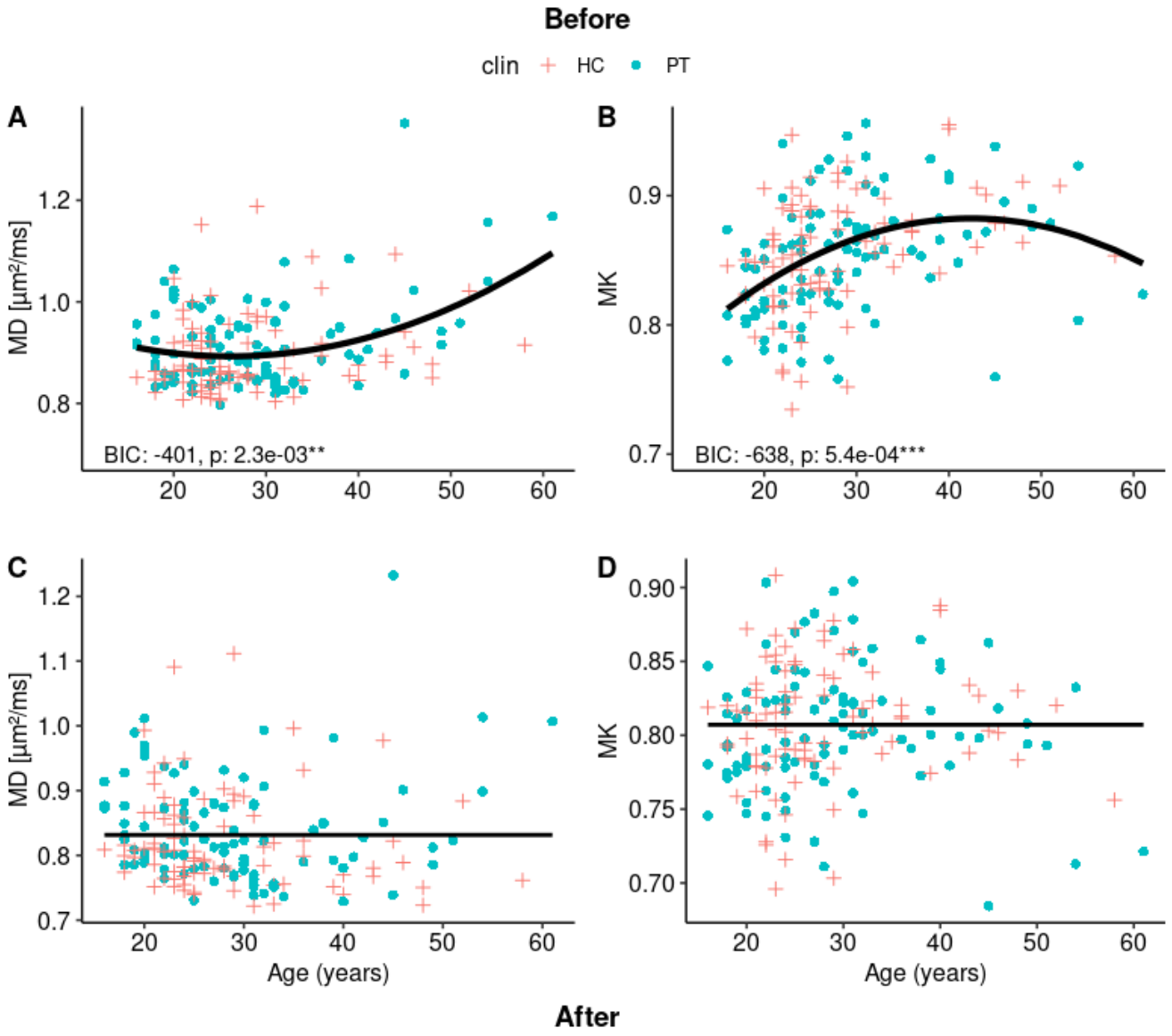

Figure S 3: Before (A, B) vs after (C, D) examples of fits for the best age correction model of the WM skeleton MD (A, C) and MK (B, D). The procedure selected the quadratic age effect (QAE) as best model. In the before-plots (A, B), the black solid line indicates the predicted values of MD or MK given the corresponding age. In the after age correction plots (C, D), the model intercept is maintained and just the age effect is removed.

Diagnosis

		N	Pct.
Diagnosis	Bipolar disorder	2	2.0
	Bipolar disorder with psychotic features	3	3.1
	Brief psychotic disorder	8	8.2
	Cannabis-induced psychotic disorder	1	1.0
	Delusional disorder	1	1.0
	Schizoaffective disorder	8	8.2
	Schizophrenia	65	66.3
	Schizophreniform disorder	9	9.2
	Unspecified psychotic disorder; Depressive disorder	1	1.0

Table S 1: Patients individual diagnosis. Pct. Percentage

References

Y. Alemán-Gómez, T. Baumgartner, P. Klauser, M. Cleusix, R. Jenni, P. Hagmann, P. Conus, K. Q. Do, M. Bach Cuadra, P. S. Baumann, and P. Steullet. Multimodal Magnetic Resonance Imaging Depicts Widespread and Subregion Specific Anomalies in the Thalamus of Early-Psychosis and Chronic Schizophrenia Patients. *Schizophrenia Bulletin*, 49(1):196–207, Jan. 2023. ISSN 0586-7614. doi: 10.1093/schbul/sbac113. URL https://doi.org/10.1093/schbul/sbac113.

J. L. R. Andersson and S. N. Sotiropoulos. An integrated approach to correction for off-resonance effects and subject movement in diffusion MR imaging. *NeuroImage*, 125:1063–1078, Jan. 2016. ISSN 1095-9572. doi: 10.1016/j.neuroimage.2015.10.019.

M. Bastiani, M. Cottaar, S. P. Fitzgibbon, S. Suri, F. Alfaro-Almagro, S. N. Sotiropoulos, S. Jbabdi, and J. L. R. Andersson. Automated quality control for within and between studies diffusion MRI data using a non-parametric framework for movement and distortion correction. *NeuroImage*, 184:801–812, Jan. 2019. ISSN 1095-9572. doi: 10.1016/j.neuroimage.2018.09.073.

E. Kellner, B. Dhital, V. G. Kiselev, and M. Reisert. Gibbs-ringing artifact removal based on local subvoxel-shifts. *Magnetic Resonance in Medicine*, 76(5):1574–1581, 2016. ISSN 1522-2594. doi: 10.1002/mrm.26054. URL https://onlinelibrary.wiley.com/doi/abs/10.1002/mrm.26054. _eprint: https://onlinelibrary.wiley.com/doi/pdf/10.1002/mrm.26054.

H.-H. Lee, D. S. Novikov, and E. Fieremans. Removal of partial Fourier-induced Gibbs (RPG) ringing artifacts in MRI. *Magnetic Resonance in Medicine*, 86(5):2733–2750, 2021. ISSN 1522-2594. doi: 10.1002/mrm.28830. URL https://onlinelibrary.wiley.com/doi/abs/10.1002/mrm.28830. _eprint: https://onlinelibrary.wiley.com/doi/pdf/10.1002/mrm.28830.

J. T. Leek, W. E. Johnson, H. S. Parker, A. E. Jaffe, and J. D. Storey. The sva package for removing batch effects and other unwanted variation in high-throughput experiments. *Bioinformatics*, 28(6):882–883, Mar. 2012. ISSN 1367-4803. doi: 10.1093/bioinformatics/bts034. URL https://www.ncbi.nlm.nih.gov/pmc/articles/PMC3307112/.

R Core Team. *R: A Language and Environment for Statistical Computing*. R Foundation for Statistical Computing, Vienna, Austria, 2023. URL https://www.R-project.org/.

C. M. W. Tax, M. Bastiani, J. Veraart, E. Garyfallidis, and M. Okan Irfanoglu. What's new and what's next in diffusion MRI preprocessing. *NeuroImage*, 249:118830, Apr. 2022. ISSN 1053-8119. doi: 10.1016/j.neuroimage.2021.118830. URL https://www.sciencedirect.com/science/article/pii/S1053811921011010.

J. Veraart, D. S. Novikov, D. Christiaens, B. Ades-Aron, J. Sijbers, and E. Fieremans. Denoising of diffusion MRI using random matrix theory. *NeuroImage*, 142:394–406, Nov. 2016. ISSN 1095-9572. doi: 10.1016/j.neuroimage.2016.08.016.